Polymorphous silicon thin films obtained by plasma-enhanced chemical vapor deposition using dichlorosilane as silicon precursor

2009 Nanotechnology 20 245604

(http://iopscience.iop.org/0957-4484/20/24/245604)

Nanotechnology **20** (2009) 245604 (6pp) doi:10.1088/0957-4484/20/24/245604

Polymorphous silicon thin films obtained by plasma-enhanced chemical vapor deposition using dichlorosilane as silicon precursor

A Remolina[1], B M Monroy[1], M F García-Sánchez[1], A Ponce[2], M Bizarro[1], J C Alonso[1], A Ortiz[1] and G Santana[1,3]

[1] Instituto de Investigaciones en Materiales, Universidad Nacional Autónoma de México, AP 70-360, Coyoacán, CP 04510, DF, Mexico
[2] Centro de Investigación en Química Aplicada, Boulevard Enrique Reyna Hermosillo # 140, CP 25290, Saltillo, Coahuila, Mexico

E-mail: gsantana@iim.unam.mx

Received 27 February 2009, in final form 19 April 2009
Published 27 May 2009
Online at stacks.iop.org/Nano/20/245604

Abstract
Polymorphous silicon thin films (pm-Si) have been deposited from mixtures of dichlorosilane and hydrogen, using argon as the diluting gas by plasma-enhanced chemical vapor deposition. The deposition conditions were chosen to simultaneously obtain both Si nanocrystallites and an amorphous silicon matrix in the as-grown samples. High resolution transmission electron microscopy studies show the crystallinity of Si domains whose dimensions are in the interval of 2–14 nm. The surface passivation state of the silicon nanocrystals was inferred from Fourier transform infrared spectroscopy analysis. Two optical absorption edges, corresponding to the amorphous matrix and the Si nanocrystals, were observed for all the pm-Si thin films. Intense visible photoluminescence was observed for the as-grown samples. The possibility of using these thin films for the down-conversion effect in silicon solar cells is discussed.

(Some figures in this article are in colour only in the electronic version)

1. Introduction

Polymorphous silicon (pm-Si) thin films are promising structures for a wide range of applications in micro- and optoelectronics (solar cells, flat panel display applications, thin film transistors, etc) [1, 2]. Polymorphous silicon thin films with nanocrystalline silicon inclusions, pm (nc-Si:H), have received considerable attention due to reports of electronic properties comparable to those of hydrogenated amorphous silicon (a-Si:H) with the advantage of a better resistance to the formation of light-induced defects. This material has steadily emerged as a potential replacement of a-Si:H in a variety of applications, in particular for photovoltaics, because of the improved properties, such as the excellent thermal, chemical and photostability of pm-Si with respect to standard a-Si:H.

[3] Author to whom any correspondence should be addressed.

Plasma-enhanced chemical vapor deposition (PECVD) is one of the promising methods for the growth of Si-based thin films [3, 4], owing to its capability of performing low-temperature processes, the ease of depositing a large area film and its compatibility with the a-Si:H technology. Besides, the optical and electrical properties of pm-Si:H can be controlled readily by the growth parameters during the PECVD process [1–6].

Hydrogenated polymorphous silicon films have been deposited mostly by using highly diluted silane in hydrogen mixtures [3–6]. However, the use of high hydrogen dilutions during the PECVD process can contribute to an excessive incorporation of weak Si–H bonds into the pm-Si films. This, in turn, results in the degradation of the optoelectronic properties of the films after prolonged illumination which leads to deterioration of the material quality [4]. Another drawback of the use of high hydrogen dilutions in the PECVD process is

Table 1. Growth conditions and thicknesses of pm-Si samples.

Sample	RF power (W)	R (SiH_2Cl_2/H_2)	Thickness (nm) (±5 nm)	Growth rates (Å s^{-1})
pm_si001	50	0.05	118	0.6
pm_si002	100	0.05	134	0.7
pm_si004	50	0.1	157	0.8
pm_si006	150	0.1	169	0.9

the surface erosion produced by atomic hydrogen. This effect could deteriorate the interface between the pm-Si film and the substrate, which would be prejudicial to integrated device performance [1].

Recently, we have observed that the use of dichlorosilane as precursor gas in the PECVD process introduces the possibility of obtaining nanocrystalline silicon inclusions in an amorphous matrix at low deposition temperatures and without the need of thermal annealing [7–9]. The interaction between the growing surface and reactive hydride and chloride radicals present in the hydrogen-rich plasma results in films that are a mixture of an amorphous matrix and different crystalline silicon formations (nc-Si and μc-Si), depending on the deposition conditions.

In this work, polymorphous silicon is obtained using dichlorosilane as a silicon precursor gas in the PECVD process. The deposition conditions were chosen to favor the as-grown deposition of nanocrystalline silicon inclusions with the aim of relating the deposition plasma characteristics to the structural and optical properties of the films. The possibility to use these thin films for the down-conversion effect in silicon solar cells was evaluated by photoluminescence and absorbance measurements.

2. Experimental procedure

The pm-Si thin films were prepared using a conventional PECVD system with parallel plates of 150 cm^2 in area and 1.5 cm apart, activated by a 13.56 MHz RF signal. The system is described in more detail elsewhere [10]. The films were deposited on quartz, NaCl and high resistivity crystalline silicon (n-type, ⟨100⟩) substrates. Prior to deposition, the substrates were subjected to a standard cleaning procedure, which included 1 min etching in diluted hydrofluoric acid (5% HF) to remove the surface native oxide on the silicon substrate, immediately before loading them into the deposition chamber. Ultrahigh purity Ar, SiH_2Cl_2 and H_2 were used as precursor gases. In all cases the substrate temperature was kept constant at 200 °C and an argon flow rate of 50 sccm was used as diluent gas. The deposition time and pressure were fixed at 30 min and 250 mTorr, respectively. Plasma powers of 50, 100 and 150 W were tested. Two different $[SiH_2Cl_2]/[H_2]$ flow rate ratios (R) were used, 0.05 and 0.1, while the hydrogen flow was fixed at 50 sccm in all cases. The deposition conditions and film thickness of the studied samples are summarized in table 1.

The optical properties of the films were analyzed by photoluminescence (PL) and UV–vis transmittance spectra. PL measurements were carried out at room temperature, using an excitation wavelength of 325 nm and a power of 20 mW from an He–Cd KIMMON™ laser. The PL signal was collected with an optical fiber and analyzed in a Spex-Fluoromax spectrofluorometer. Transmittance measurements were recorded in a UV–vis spectrometer UNICAM 3000 and the optical gap was calculated by the method of Tauc plotting. The thickness of the films was determined by a Sloan Dektak IIA surface profile measuring system.

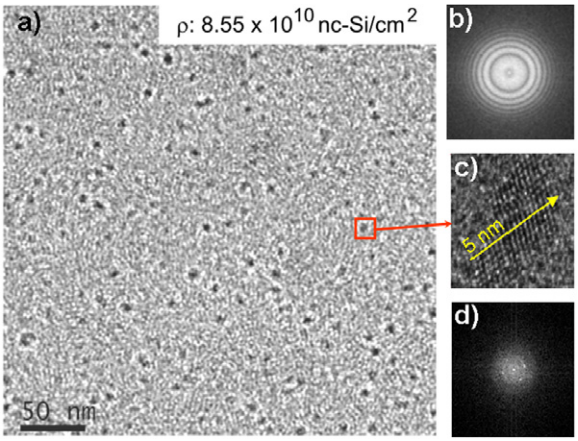

Figure 1. (a) HRTEM micrograph showing the nc-Si embedded in the amorphous silicon matrix obtained for a pm-Si film deposited with an $R = 0.05$ flow rate ratio and an RF power of 50 W. (b) Electron diffraction pattern of the pm-Si film dominated by the amorphous silicon matrix. (c) Zoom showing the crystalline structure of an oval silicon domain. (d) Fourier transform of (c) showing the corresponding crystalline directions.

The chemical bonding of the films was analyzed by Fourier transform infrared spectroscopy (FTIR). The measurements were performed on a FTIR Nicolet Nexus 670. To observe the films' microstructure, high resolution transmission electron microscopy (HRTEM) studies were conducted in a JEM-2010F microscope, operated at 200 kV. The images were obtained in the Scherzer focus and recorded simultaneously online with a CCD camera. The Gatan DigitalMicrograph™ software was used for analysis of the HRTEM images. It is important to notice that the sample for HRTEM analysis was deposited over an NaCl substrate. The substrate was then dissolved in distilled water and the film was collected on a Cu grid. In this way we ensured that no modification of the film structure is produced, as could be the case in conventional ion milling techniques used to prepare samples for HRTEM.

3. Results and discussion

3.1. HRTEM

Figure 1 shows an HRTEM image obtained for a pm-Si film deposited with an $R = 0.05$ flow rate ratio and a RF power of 50 W. The presence of silicon nanocrystals (nc-Si) in the film can be observed in figure 1(a). The density of nc-Si in this image is 8.55×10^{10} cm^{-2}. Figure 1(b) shows the electron diffraction pattern of the film in the same area as shown in figure 1(a). The concentric rings show an amorphous structure associated with the matrix. The sizes of the nanocrystalline Si

domains are between 2 and 14 nm. To show the crystallinity of the silicon inclusions, figure 1(c) presents a zoom into an oval silicon structure. The Gatan DigitalMicrograph™ software was used to calculate the interplanar distance in the direction of the arrow shown in the image. The measured distance was $d_{(hkl)} = 0.312$ nm, which corresponds to (111) planes in crystalline silicon. The estimated lattice parameter is 0.540 nm which is in good agreement with the reported lattice parameter of crystalline silicon. The Fourier transform of figure 1(c) is shown in (d), further confirming the crystalline structure of the inclusion. This combination of amorphous matrix and nanocrystalline inclusions was obtained for all the pm-Si films discussed in this work without any kind of post-deposition treatment.

3.2. FTIR spectroscopy

Figure 2 shows typical IR absorption spectra acquired for all samples in the regions from 400 to 850 cm^{-1} and from 1500 to 2400 cm^{-1}. The region from 400 to 850 cm^{-1} shows two principal absorption bands centered around 620–630 cm^{-1} and 710–730 cm^{-1}. These bands are associated with Si_mH_n wagging vibration modes. The small shifts observed in the position of these peaks are associated with stress in the Si_mH_n bonding configuration [4, 11]. It should be noted that these bands are very intense and they appear in all the analyzed samples. On the other hand, the stretching vibration mode corresponding to Si–H mono- and dihydride bonding type, which should occur between 2000 and 2150 cm^{-1}, was not observed, indicating that their concentration is below the limit of detection (1%) [12]. These Si–H bonding types are generally present in the amorphous silicon matrix of pm-Si films and they are held responsible for the degradation of the electrical properties of the amorphous silicon devices.

The chlorine chemistry introduced in the PECVD processes by means of the silicon precursor (SiH_2Cl_2) generates important differences regarding the films' properties in comparison to the widely used silane (SiH_4). The most remarkable issues derived from the use of chlorinated precursors are: (i) the enhanced reactivity of SiH_xCl_y species in the plasma can stimulate secondary reactions in the gas phase (even for relatively low hydrogen dilutions) that lead to the formation and growth of silicon nanocrystals (nc-Si) in the plasma [2, 3, 12, 13]. Thus, the increase of the SiH_2Cl_2 flow rate (from 2.5 to 5 sccm) in the gas mixture as well as of the RF power (from 50 to 150 W) can increase the concentration of reactive species and stimulate these secondary reactions in the gas phase, causing the plasma conditions to be close to powder formation [1]. (ii) Metastable $SiCl_xH_y$ precursors that incorporate into the surface are highly reactive with impinging atomic hydrogen. This promotes exothermic reactions that lead to the formation of HCl. These reactions cause a local heating that enhances crystallization of the nc-Si at low deposition temperatures [13, 14]. In this way the chlorine chemistry introduced in the PECVD process enhances the formation of crystalline silicon regions without the need for thermal annealing. It can also be inferred that this process acts as a regulator of the metastable hydrogen and chlorine incorporation into the pm-Si films. (iii) Chlorine acts as a terminal bond in the surface of Si due to the stability of the Si–Cl bond (391 kJ mol^{-1}). The probability of breaking these bonds during the deposition process is smaller than the probability of breaking weaker monohydride Si–H (328 kJ mol^{-1}) and Si–Si (226 kJ mol^{-1}) bonds. Thus, Si–Cl bonds limit the nc-Si size, as has been discussed in previous works [13]. As Cl forms terminal bonds, the films resulting with a high Cl content are expected to have an open (porous) structure. This statement is supported by the SEM images reported elsewhere [13]. The excess of Cl incorporated into the network also lowers the film's chemical stability.

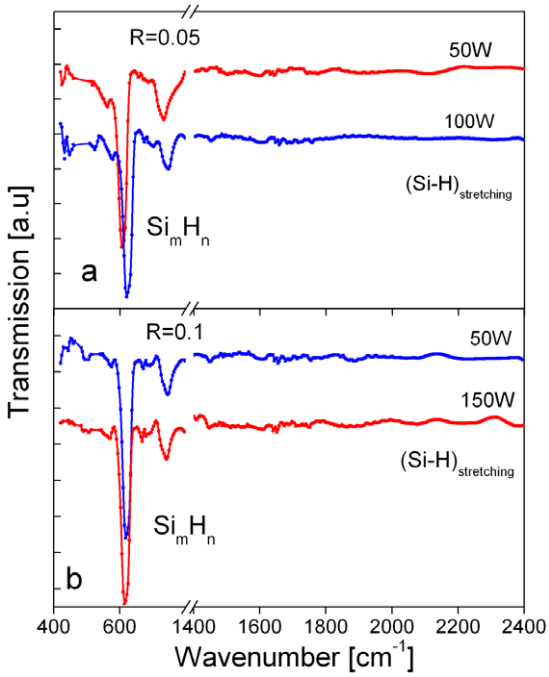

Figure 2. FTIR spectra of the samples deposited with: (a) 50 and 100 W of RF power and $R = 0.05$ and (b) 50 and 150 W of RF power and $R = 0.1$.

The FTIR results observed in figure 2 can be explained in terms of the chlorine chemistry discussed previously. The absence of mono-and dihydride Si–H bonds around 2000–2150 cm^{-1} can be due to the HCl extraction process. These bonds are generally weak and metastable and therefore prone to react with chlorine-related species. On the other hand, hydrogen bonds present in the surface of the nanocrystalline silicon inclusions in the a-Si matrix contribute to the stability of the structure, as has been shown in a number of theoretical works [11, 15]. Therefore the Si_mH_n bonding configurations are more stable than the hydrogen bonded weakly to the a-Si:H matrix. Furthermore, in previous works the modes around 600–730 cm^{-1} have been related to the surface passivation of the nanocrystals that are embedded in the amorphous silicon matrix [7, 11, 16–18]. Based on these observations we believe that the hydrogen bonding in the films mainly passivates the nanoclusters' surface in the interfaces between the amorphous matrix and the silicon nanocrystals. Besides, the hydrogen

used in the PECVD process also extracts metastable chlorine from the films, contributing to their chemical stability. For example, the FTIR spectra of the films grown at $R = 0.05$ and 50 watts of RF power remained unchanged after months of ambient exposure. Furthermore, in all the analyzed samples the stretching vibration mode corresponding to Si–Cl bonding is not observed at 545 cm^{-1}, indicating the low chlorine content of the films (less than 1%) [14, 19].

3.3. UV–visible absorbance spectroscopy

The optical bandgap (E_g^{op}) of the films was calculated from absorbance measurements by the method of Tauc plotting [7, 20]. In this method $(\alpha h\nu)^{1/2}$ is plotted versus $h\nu$, where α is the absorption coefficient of the film, h is the Planck constant and ν is the frequency of light. Then, a linear regression is performed in the region around the absorption edge where $(\alpha h\nu)^{1/2}$ is proportional to $h\nu$. The energy-axis intercept of this line is associated with the optical bandgap E_g^{op}. With this approximation, an effective optical bandgap is obtained that is representative of the whole material.

Tauc plots of the samples grown onto fused silica substrates are displayed in figure 3. In all samples two distinct absorption edges can be observed. The linear regressions that were made for the data introduce an error in the calculated bandgaps of ±0.01 eV. The bandgap located around 1.5–1.9 eV was associated with the amorphous silicon matrix. The changes in E_g^{op} depend on the form and content of hydrogen bonding in the a-Si:H films, as has been reported previously [21]. On the other hand, the higher energy bandgap (2.0–2.7 eV) can be associated with the nc-Si. This bandgap suffers a redshift as a function of the dichlorosilane to hydrogen flow rate ratio, $R = [SiH_2Cl_2/H_2]$. Comparing the different curves shown in figure 2, it can be observed that, when R increases from 0.05 to 0.10, the optical bandgap decreases from 2.7 and 2.45 eV to 2.23 to 2.03 eV. The bandgap shows a different behavior as a function of the RF power since it redshifts for $R = 0.05$ and it blueshifts for $R = 0.10$.

One way to explain the shift in the optical bandgaps when the deposition conditions are changed is to associate this redshift with an increase of the nc-Si average size when R increases or the RF power is increased at $R = 0.05$. According to quantum confinement theory the optical bandgap E_{op} depends on the size of the nc-Si. The confinement model proposed by Trwoga *et al* [22] for silicon nanoclusters is

$$E_{op} = E_g + \frac{c}{a^2} \quad (1)$$

where c is the confinement constant, E_g is the bulk silicon bandgap and a is the nanocluster diameter.

An increase in the nc-Si size depending on the deposition conditions is compatible with previous observations where the average size of silicon nanocrystals is controlled by the parameters used in the PECVD process [7, 9, 23]. In our case, an increase in the RF power at $R = 0.05$ produces more atomic hydrogen during the deposition. The presence of atomic hydrogen plays an important role in the creation of nucleation sites in the surface by breaking weak bonds or reacting with chlorine-related species and leaving a dangling bond after the HCl extraction. Along with the local heating induced by this process, this leads to an increment in size and density of the crystalline regions that are formed during the deposition and it can even enhance the agglomeration of adjacent nc-Si during growth. Thus, for this deposition condition bigger nc-Si are formed and the optical absorption edge shifts towards lower energies.

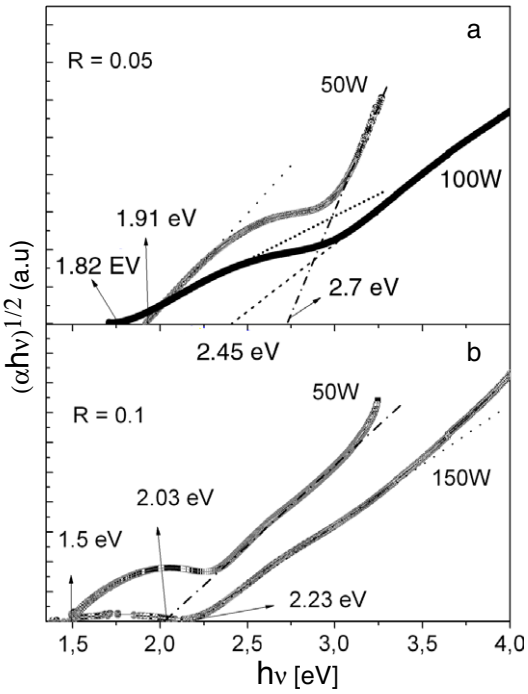

Figure 3. Optical bandgaps obtained by the Tauc plotting method of samples deposited with the following conditions: (a) $R = 0.05$ and RF powers of 50 and 100 W, (b) $R = 0.1$ and RF powers of 50 and 150 W.

For the sample deposited with $R = 0.10$ and an RF power of 150 W most of the nanocrystalline inclusions were bigger than 10 nm. The quantum confinement effects can only be appreciated for nc-Si with dimensions smaller than 10 nm where the exciton radius is less than the Bohr radius for crystalline silicon [22]. Therefore, only the nanocrystalline inclusions with dimensions smaller than 10 nm follow the model expressed by equation (1). Thus, the effective bandgap obtained for the sample deposited in these conditions does not follow the trends observed for the others presented in figure 3.

3.4. Photoluminescence

Like the optical bandgap, the photoluminescence (PL) also depends on the deposition conditions [7, 8]. Figure 4 shows the different PL spectra corresponding to as-grown samples deposited under the conditions specified in table 1. It is important to emphasize that visible and strong photoluminescence at room temperature was obtained from the samples without any thermal annealing. The strong emission could be seen with the naked eye and lights turned on in the laboratory. The inset spot images on figures 4(a) and (d)

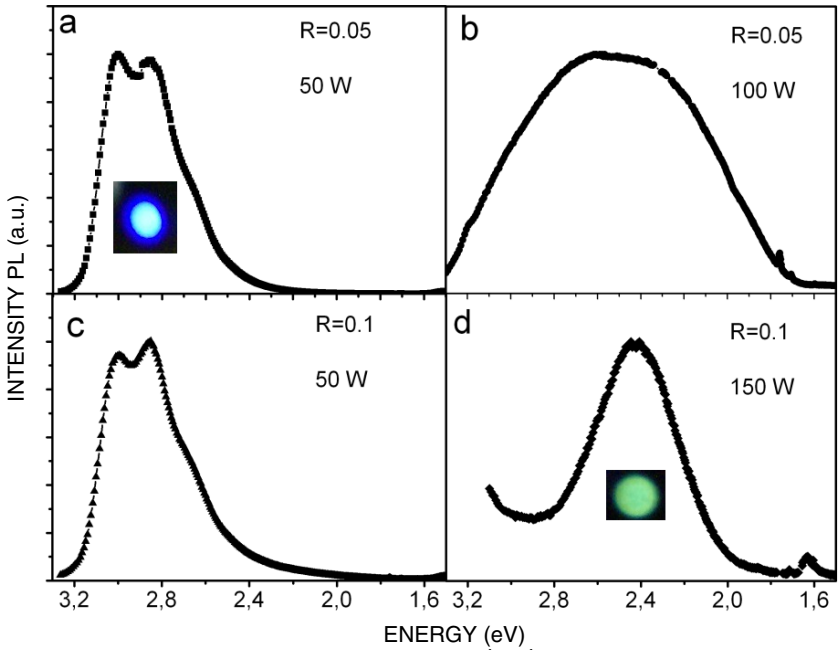

Figure 4. PL spectra of samples deposited with: (a) 50 W RF power and $R = 0.05$, (b) 100 W RF power and $R = 0.05$, (c) 50 W RF power and $R = 0.10$ and (d) 150 W RF power and $R = 0.10$.

correspond to photographs taken with a standard digital camera during the PL measurements.

In figure 4(a) the sample was deposited at 50 W RF power and $R = 0.05$. The PL consists of a band between 2.2 and 3.3 eV. Increasing the RF power from 50 to 100 W, keeping the same R, causes a marked increase in the width of the PL band (figure 4(b)). Figure 4(c) presents a PL emission very similar to figure 4(a). In this case both samples were deposited at 50 W RF power but with different R (0.05 for the sample in 4(a) and 0.10 for the sample in 4(c)). Increasing the RF power to 150 W with $R = 0.10$ (figure 4(d)) produces a Gaussian-like peak around 2.42 eV.

According to theoretical models of quantum confinement, PL in the visible region can only be obtained from silicon nanoclusters with diameters less than 10 nm. The quantum confinement model has been used in previous works that compare experimental and theoretical PL data from silicon nanoclusters embedded in amorphous matrices showing that the correlation between the two results is excellent [12, 17, 22, 23]. Thus, according to the model proposed by Trwoga *et al* [22], the shift and form of the PL peak depends on the average size and size distribution of the silicon nanocrystals embedded in the a-Si:H matrix with dimensions smaller than 10 nm that can contribute to the observed PL emission.

As a consequence, the observed PL redshift with increasing RF power shown in figure 4 can be associated with larger nc-Si formed in the amorphous silicon matrix with this deposition conditions. This result is completely consistent with the observed optical absorption trends discussed in section 3.3. The optical bandgap also decreases (redshifts) with increasing RF power at $R = 0.05$. This is an expected result since both the optical absorption and emission are associated with quantum confinement effects in the nc-Si.

From figures 4(a) and (b), it can be inferred that increasing the RF power also causes a broader size distribution (associated with the form of the PL spectrum) of nc-Si during deposition. Again, this can be explained in terms of the atomic hydrogen abundance in the PECVD increased by the RF power. The increment of nc-Si nucleation sites, HCl extraction reactions and local heating with RF power is expected to cause a broader nc-Si size distribution during the deposition process. In contrast, keeping the RF power fixed at 50 W and increasing R (figures 4(a) and (c)) produces almost the same average size of small nc-Si formed in the as-grown samples. The multi-peak spectra can be associated with a non-Gaussian size distribution of nc-Si as has been observed in previous works where a detailed HRTEM measurement of the nc-Si size distribution was made [13, 24]. Even though the SiH_2Cl_2 flow rate ratio was increased for the samples corresponding to figures 4(a) and (c), the hydrogen dilution was kept constant ($Fr[H_2] = 50$ sccm in all cases). At a fixed RF power the ionization rate in the plasma is constant. Therefore the atomic hydrogen generated during the deposition of these two samples was very similar. Since this atomic hydrogen is determinant for the nc-Si formation in the a-Si:H matrix it is not surprising that PL spectra in figures 4(a) and (c) are so close.

The intense PL emission of the samples can be attributed to the passivation of the nanocrystal's surface. The intense FTIR bands corresponding to Si_mH_n wagging modes can be an indicator that the surface passivation of the nc-Si is stable since the spectra did not change after months of ambient exposure. This stable surface passivation is important for the PL intensity since the presence of surface defects or dangling bonds would increase the non-radiative recombination mechanisms. Also, an improved surface passivation gives greater chemical stability to the film [9]. This condition was confirmed from

FTIR measurements and the fact that the PL emission and optical absorption were all the same months after deposition.

Based on these results, we can propose the pm-Si thin films with small nanocrystals embedded in the amorphous silicon matrix as a promising candidate for a material that could act as a photon frequency converter (down-converter). In the down-conversion (DC) effect it is possible that incident high energy photons are transformed by the luminescent material into two or more lower energy photons [25–27]. In the case of photovoltaic applications, the passive luminescent layer shifts incident high energy photons towards lower energies for which the solar cell works more efficiently. For our samples, the DC occurs from the ultraviolet wavelength (PL excitation = 325 nm) to the visible (emission spectra).

It is important to notice that the solar cell and the luminescence layer can be independent layers separated by an insulator, for example [27]. In this way, the two constituents of the system can be optimized separately with different materials. This is advantageous, because fairly different requirements must be met for an efficient luminescence converter and for an efficient solar cell material, respectively. For instance the transport properties and the luminescent properties can be very different in the solar cell and the luminescent layer. In addition, the application of DC layers does not require modification of the existing solar cell as the layers are passive and purely optical in operation [26]. Therefore the pm-Si films studied in this work have the potential to be used as down-conversion material in silicon solar cells or in heterojunctions with intrinsic thin layer (HIT) solar cells.

4. Conclusions

We have demonstrated that a polymorphous silicon material was obtained starting from dichlorosilane as a silicon precursor. The chlorine chemistry introduced by the silicon precursor favors the formation of nanocrystalline inclusions without the need of post-deposition treatments. The hydrogen bonding configuration of the films corresponds mainly to Si_mH_n modes that are associated with the surface passivation of the silicon nanocrystals. Visible and strong photoluminescence (PL) at room temperature was obtained from polymorphous silicon thin films with nanocrystalline inclusions. The PL emission was observed with the naked eye in all the analyzed samples. The optical bandgap and the PL peak of these polymorphous materials can be varied as a function of the growth parameters. PL results show conversion of photon frequency from UV to visible. The structural features and optical properties of the films show a very stable performance, as evidenced from FTIR, PL and UV–vis measurements months after deposition. Based on these results, we propose the pm-Si thin films with small nanocrystals as a promising candidate for a material that could act as a down-converter in solar cells.

Acknowledgments

We acknowledge partial financial support for this work from CONACyT México, under project 48970 and PAPIIT-UNAM under projects IN116409-2 and IN115909-2. AR expresses thanks for the scholarship grant by CLAF-Brasil and ICyTDF-México DF.

References

[1] Roca i Cabarrocas P, Fontcuberta i Morral A and Poissant Y 2002 *Thin Solid Films* **403/404** 39–46
[2] Roca i Cabarrocas P 2000 *J. Non-Cryst. Solids* **266–269** 31–7
[3] Poissant Y, Chatterjee P and Roca i Cabarrocas P 2002 *J. Non-Cryst. Solids* **299–302** 1173–8
[4] Saadane O, Lebib S, Kharchenko A V, Longeaud C and Roca i Cabarrocas P 2003 *J. Appl. Phys.* **93** 9371–9
[5] Vignoli S, Butté R, Meaudre R, Meaudre M and Roca i Cabarrocas P 1999 *J. Phys.: Condens. Matter* **11** 8749–57
[6] Li S B, Wu Z M, Li W, Liao N M and Jiang Y D 2007 *Phil. Mag.* **87** 5539–49
[7] Monroy B M, Santana G, Aguilar-Hernández J, Benami A, Fandiño J, Ponce A, Contreras-Puente G, Ortíz A and Alonso J C 2006 *J. Lumin.* **121** 349–52
[8] Santana G, Monroy B M, Ortíz A, Huerta L and Alonso J C 2006 *Appl. Phys. Lett.* **88** 041916
[9] Benami A, Santana G, Ortiz A, Ponce A, Romeu D, Aguilar-Hernández J, Contreras-Puente G and Alonso J C 2007 *Nanotechnology* **18** 155704
[10] Santana G, Fandiño J, Ortiz A and Alonso J C 2005 *J. Non-Cryst. Solids* **351** 922–8
[11] Kopáni M, Pincik E, Kobayashi H, Takahashi M, Fujiwara N, Brunner R, Jergel M and Ortega L 2006 *Appl. Surf. Sci.* **252** 7722–5
[12] Chang C Y and Sze S M 2000 *ULSI Technology* (New York: Wiley)
[13] Monroy B M *et al* 2009 *J. Nanosci. Nanotechnol.* **9** 2902–9
[14] Liu H, Jung S, Fukimura Y, Fukai C, Shirai H and Toyoshima Y 2001 *Japan. J. Appl. Phys.* **40** 44–8
[15] Vach H, Brulin Q, Chaâbane N, Novikova T, Roca i Cabarrocas P, Kalache B, Hassouni K, Botti S and Reining L 2006 *Comput. Mater. Sci.* **35** 216–22
[16] Lucovsky G, Yang J, Chao S S, Tyler J E and Czubatyj W 1983 *Phys. Rev.* B **28** 3225–33
[17] Mullerová J, Jurecka S and Sutta P 2006 *Sol. Energy* **80** 667–74
[18] Ali A M 2007 *J. Lumin.* **126** 614–22
[19] Hashimoto K and Shirai H 2003 *Japan. J. Appl. Phys.* **42** 1173–8
[20] Wood D L and Tauc J 1972 *Phys. Rev.* B **5** 3144–51
[21] Futako W, Kamiya T, Fortmann C M and Shimizu I 2000 *J. Non-Cryst. Solids* **266–269** 630–4
[22] Trwoga P F, Kenyon A J and Pitt C W 1998 *J. Appl. Phys.* **83** 3789–94
[23] Kim T-Y, Park N-M, Kim K-H, Sung G Y, Ok Y-W, Seong T-Y and Choi C-J 2004 *Appl. Phys. Lett.* **85** 5355–7
[24] Ponce A, Benami A, Santana G, Alonso J C, Aguilar-Hernández J, Contreras-Puente G, Ortiz A, Fandiño J and Romeu D 2007 *Phys. Status Solidi* c **4** 1458–61
[25] Maruyama T and Kitamura R 2001 *Sol. Energy Mater. Sol. Cells* **69** 207–16
[26] Richards B S 2006 *Sol. Energy Mater. Sol. Cells* **90** 2329–37
[27] Trupke T, Würfel P and Green M A 2003 *Proc. 3rd World Conf. on Photovoltaic Energy Conversion (Osaka)* vol 1 (Japan: WCPEC-3 Organizing Committee) pp 67–70